RESEARCH ARTICLE | MAY 25 2023

## Spin-orbit effects on the electronic and optical properties of lead iodide $\odot$

Woncheol Lee <sup>(i)</sup>; Zhengyang Lyu <sup>(i)</sup>; Zidong Li <sup>(i)</sup>; Parag B. Deotare <sup>(i)</sup>; Emmanouil Kioupakis <sup>(i)</sup>



Appl. Phys. Lett. 122, 212110 (2023) https://doi.org/10.1063/5.0146397





CrossMark

#### Articles You May Be Interested In

Band gap engineering of a soft inorganic compound  $\mathrm{Pbl}_2$  by incommensurate van der Waals epitaxy

Appl. Phys. Lett. (January 2016)

Semiconductor-metal transition in lead iodide under pressure

Appl. Phys. Lett. (May 2022)

Purely physical fabrication of 10 cm  $\times$  10 cm, highly uniform PbI<sub>2</sub> thin films on rigid and flexible substrates for x-ray photodetection application

APL Mater (March 2020)

500 kHz or 8.5 GHz? And all the ranges in between.

Lock-in Amplifiers for your periodic signal measurement









# Spin-orbit effects on the electronic and optical properties of lead iodide

Cite as: Appl. Phys. Lett. **122**, 212110 (2023); doi: 10.1063/5.0146397 Submitted: 13 February 2023 · Accepted: 12 May 2023 · Published Online: 25 May 2023









#### **AFFILIATIONS**

- <sup>1</sup>Department of Electrical and Computer Engineering, University of Michigan, 1301 Beal Avenue, Ann Arbor, Michigan 48109, USA
- <sup>2</sup>Applied Physics Program, University of Michigan, 450 Church St., 1425 Randall Laboratory, Ann Arbor, Michigan 48109, USA

#### **ABSTRACT**

Lead iodide (PbI<sub>2</sub>) has gained much interest due to its direct electronic gap in the visible range and layered crystal structure. It has thereby been considered as a promising material for applications in atomically thin optoelectronic devices. In this work, we present a detailed investigation of the effect of spin–orbit coupling (SOC) that arises from the presence of heavy atoms on the electronic and optical properties of PbI<sub>2</sub> using first-principles calculations based on density-functional theory and many-body perturbation theory. We find that SOC not only alters the bandgap but also induces the mixing of orbital characters, resulting in a significant change in the overall band structure and charge carrier effective masses. Moreover, the band orbital mixing caused by SOC results in the dramatic change in optical transition matrix elements and, correspondingly, the absorption spectrum. Our experimentally measured absorption spectra validate the calculation results and demonstrate the importance of SOC in the optical processes of PbI<sub>2</sub>. Our findings provide insights that are important for the potential use of PbI<sub>2</sub> as a material platform for visible optoelectronic devices.

Published under an exclusive license by AIP Publishing. https://doi.org/10.1063/5.0146397

Lead iodide (PbI<sub>2</sub>) is a layered semiconductor, where covalently bonded triatomic layers (I–Pb–I) are stacked by van der Waals (vdW) interactions. PbI<sub>2</sub> is known to exhibit a direct bandgap in the visible range, allowing its wide applications in high-performance optoelectronic devices, such as lasers and photodetectors. Also, due to its ability to react with amine iodides, PbI<sub>2</sub> has gained immense popularity as a precursor for halide perovskites, which has widely been explored for high-efficiency light-emitting diodes and photovoltaic devices. Furthermore, the nature of vdW interaction allows PbI<sub>2</sub> to form various types of heterostructures with other vdW materials, such as graphene and transition metal dichalcogenides (TMDCs). These heterostructures allow us to exploit a broader range of physical phenomena, such as interlayer excitons and high spin-polarizations. 10,111

Over the past few decades, both theoretical and experimental studies have been playing an important role in deepening our understanding of the material properties of PbI<sub>2</sub>. Early studies on PbI<sub>2</sub> revealed a strong spin–orbit coupling (SOC) in this material, which is attributed to the presence of heavy elements Pb and I. <sup>12–14</sup> Later, this observation is supported by the recently developed first-principles calculation methods, which pointed out that the inclusion of the SOC is crucial for the precise calculation of the electronic properties for PbI<sub>2</sub>, indicating the strong SOC effect in PbI<sub>2</sub>. <sup>15–17</sup>

Although the prior research has improved our understanding of some of the unique features of PbI<sub>2</sub>, there is still a lack of a theoretical approach that explicitly investigates the effect of SOC on the optical properties of PbI<sub>2</sub>. SOC is known to be critically important in optical processes of various materials and systems, since it defines the orbital character of bands and the fine structure of excitons. For instance, spin-polarization is a key to understanding the unique optical properties of TMDCs, which are important for spintronic and valleytronic applications. <sup>18,19</sup> Moreover, a precise estimation of the bright-dark exciton splitting is imperative for the design of high-efficiency optoelectronic devices based on lead halide perovskites. <sup>20,21</sup> These observations firmly demonstrate the necessity of rigorous investigation of the effect of SOC in PbI<sub>2</sub>, which also has wide potential applications in the areas of photonic devices.

In this work, we investigate the electronic, optical, and excitonic properties of PbI<sub>2</sub> by fully incorporating the effect of SOC. Among many polytypes of PbI<sub>2</sub>, we focus on 2H-PbI<sub>2</sub>, which is the most common structure. We perform first-principles calculations using density functional theory (DFT) and many-body perturbation theory (MBPT). Our quasi-particle band structure calculation and band character analysis indicate that SOC mixes electron states with different orbital character and causes a huge modification in the band structure

<sup>&</sup>lt;sup>3</sup>Department of Materials Science and Engineering, University of Michigan, 2300 Hayward St., Ann Arbor, Michigan 48109, USA

a) Author to whom correspondence should be addressed: kioup@umich.edu

and carrier effective masses. In addition, the optical matrix elements calculation and the absorption calculation results support the pivotal role of SOC in the optical process of PbI<sub>2</sub>. Finally, we compare our simulated absorption spectrum with our experimentally measured spectrum and confirm that our simulation results are in good agreements with the experiments.

DFT calculations were performed within the Quantum Espresso code.<sup>22</sup> We used fully relativistic pseudopotentials and local density approximations (LDA) for the exchange-correlation functional.<sup>23</sup>, The 5*d*, 6*s*, and 6*p* electrons of Pb were included in the valence states. Two-components spinor wavefunctions were calculated on  $8 \times 8 \times 4$ Monkhorst-Pack mesh. A plane cutoff energy of 90 Ry converged the total energy to within 1mRy/atom. Using spinor wavefunctions, the quasi-particle band energy was obtained from the G<sub>0</sub>W<sub>0</sub> method, as implemented in the BerkeleyGW code.<sup>25</sup> We used the screening cutoff energy of 15 Ry and included a number of bands up to the half of the screening cutoff energy (7.5 Ry). We adopted the generalized plasmon-pole model for the calculation of frequency-dependent dielectric effects<sup>26</sup> and the static-remainder approach to increase the computation speed and achieve the better convergence of the selfenergy corrections.<sup>27</sup> Next, the quasi-particle band structure was interpolated with the maximally localized Wannier function method as implemented in the Wannier90 code.<sup>28,29</sup> Finally, using the modified dielectric matrix and quasi-particle band structure, we solved a fully relativistic form of the Bethe-Salpeter equation (BSE) to obtain excitonic properties including spin-orbit interactions. 30,31 We interpolated the Coulomb matrix elements calculated on a coarse 8 × 8 × 4 k-grid into a finer  $24 \times 24 \times 12$  k-grid using the dual-grid method, as implemented in the BerkeleyGW code.<sup>25</sup> The top four valence bands and the bottom four conduction bands were included in the BSE calculation. In addition, the scissor-shift method was applied to fix the direct bandgap at the  $\mathbf{k} = \mathbf{A}$  point to 2.52 eV.

Flakes of PbI<sub>2</sub> were mechanically exfoliated from single crystal PbI<sub>2</sub> (HQ Graphene) onto quartz substrates pretreated by oxygen plasma.<sup>32</sup> The absorption was measured using a white light source (HL-2000-LL, Ocean Insight). The white light was focused using a microscope objective and the transmitted light was collected and analyzed using a high-resolution spectrometer (IsoPlane-320 from Princeton Instruments, 300 grooves/mm grating, Pixis 400 CCD camera).

First, we calculated the quasiparticle band structure of bulk PbI<sub>2</sub> with and without SOC effects (Fig. 1). Since the s orbitals are not affected by SOC due to their zero angular momentum, we used the energies of the deep-energy bands originating from the 6s orbital of Pb atoms as a common reference to align the band structures with and without SOC effects and demonstrate the absolute effects of SOC on the higher-energy valence and conduction bands (Fig. S1). Without SOC, our calculation overestimated the direct bandgap by almost 25%  $(E_g = 3.16 \,\mathrm{eV})$ , as pointed out by previous studies. <sup>15</sup> However, we observed that accounting for SOC reduced the bandgap by almost 1 eV to a value of 2.23 eV. We also found that including the  $5s^25p^6$ core electrons of Pb atoms as valence states lead to an increase in the bandgap to 2.52 eV, which matched well with the experimentally reported electronic gap<sup>33</sup> (Table I). However, due to the extremely high computation cost of excitonic calculations with the semicore pseudopotential of Pb  $(5s^25p^65d^{10}6s^26p^3)$ , we instead used the valence pseudopotential of Pb  $(5d^{10}6s^26p^3)$  and rigidly increased the bandgap

**TABLE I.** Electronic gap of bulk Pbl<sub>2</sub> obtained from valence (5d6s6p) and semicore (5s5p5d6s6p) Pb pseudopotentials.

	w/o SOC (valence)	w/ SOC (valence)	w/ SOC (semicore)
$E_G^{DFT}$	1.98 eV	$1.24\mathrm{eV}$	1.22 eV
$E_G^{GW}$	$3.16\mathrm{eV}$	$2.23~\mathrm{eV}$	$2.52\mathrm{eV}$
$\Delta E_G^{GW}$	$1.18\mathrm{eV}$	0.99 eV	$1.30\mathrm{eV}$

by 0.29 eV to match the gap obtained with semicore pseudopotential in subsequent excitonic and optical calculations with the BSE method. Details on the comparison between the calculation results with the semicore Pb pseudopotential and the valence Pb pseudopotential is included in the supplementary material (Fig. S2).

Next, we summarize the effective mass of electrons and holes along different directions in Table II. The effective masses of electrons and holes were obtained by fitting the energy-momentum curves near the band extrema ( $\mathbf{k}=A$ ) to the parabolic equation as follows:

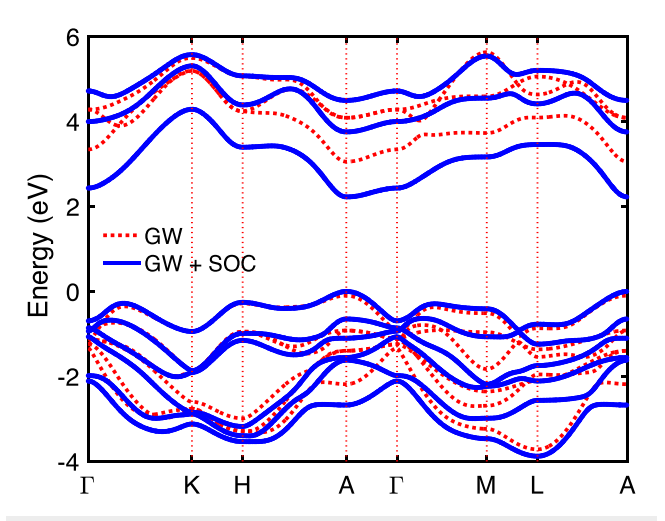


**FIG. 1.** Quasiparticle band structure of bulk Pbl<sub>2</sub> obtained from  $G_0W_0$  method using scalar-relativistic pseudopotentials (without SOC, red dashed curve) and fully relativistic pseudopotentials (with SOC, blue curve).

**TABLE II.** Effective mass of electrons and holes of bulk Pbl $_2$  in units of the free electron mass. Inclusion of SOC increases the electron effective mass parallel to the c axis  $\left(m_e^{\parallel}\right)$  and reduces the hole effective mass perpendicular to the c axis  $\left(m_h^{\perp}\right)$ .

	This work		Previous theory <sup>15</sup>	Experiments
	With SOC	Without SOC	theory	Experiments
$m_e^{\parallel}$	$1.78(A\to\Gamma)$	$1.30(A\to\Gamma)$	1.05	2.1 <sup>34</sup>
$m_e^{\perp}$	$0.26(A \to H)$	$0.26(A\to H)$	0.21	$0.48^{34}$
	$0.27(A \to L)$	$0.26(A \to L)$		
$m_h^{\parallel}$	$0.72(\mathrm{A}  o \Gamma)$	$0.68(\mathrm{A}  o \Gamma)$	0.56	$0.195^{35}$
$m_h^{\perp}$	$0.60(A\to H)$	$1.06(A\to H)$	0.59	$0.195^{35}$
	$0.62(A\to L)$	$1.11(A\to L)$		

$$E(k) = E_0 \pm \frac{\hbar^2 k^2}{2m_{e,h}},$$

where E(k) is the energy of the band at the reciprocal point k,  $E_0$  is the conduction band minimum for an electron and the valence band maximum for a hole, and  $m_{e,h}$  is an effective mass of an electron or a hole. Overall, the electron effective mass along the out-of-plane direction increases while the hole effective mass along the in-plane direction decreases with the inclusion of SOC. This change can be attributed to the mixing of band characters induced by SOC. The electron effective mass parallel and perpendicular to c-axis of PbI2 are reported to be  $m_e^{\parallel}=2.1m_0$  and  $m_e^{\perp}=0.48m_0$ .<sup>34</sup> Meanwhile, the hole effective mass was estimated to be isotropic  $(m_h = 0.195m_0)^{35}$  Our calculation that include SOC also show highly anisotropic effective masses for electrons and nearly isotropic effective masses for holes. At the same time, the predicted values are in good agreements with previous reported data. 15 We assume that the deviation of the experimental values from the simulation results can be attributed to the limit of a rough analytical approximation used in experimental data analysis. In particular, we reckon the experimental value for hole effective mass to be underestimated, due to the poor fit with the absorption peak energies. 36,37

Based on the band structure calculations, we further investigate how the SOC mixes the band character. To analyze the band character, we calculated the projected density of states (PDOS),  $\langle g_{ij}|\psi_{nk}\rangle$ , where  $g_{ij}$  is the atomic orbital i of atom j, and  $\psi_{nk}$  is the Bloch wave function for band index n and electron wave vector k. We normalized this value by the total PDOS as follows:

$$\frac{\left|\langle g_{ij}|\psi_{n\mathbf{k}}\rangle\right|^2}{\sum_{j=\mathrm{Pb,I}}\sum_{i=s,p,d}\left|\langle g_{ij}|\psi_{n\mathbf{k}}\rangle\right|^2}.$$
 (1)

This normalized PDOS value ranges from 0 to 1, indicating the orbital origin of the conduction and valence bands at each  ${\bf k}$  point. In Fig. 2, we analyzed the normalized PDOS value for the  $p_z$  orbital of Pb and I atoms, respectively, excluding SOC corrections. The figure shows that the normalized PDOS value is close to 1 only near the band extrema where  ${\bf k}={\bf A}$ . This result indicates that the  $6p_z$  orbitals of Pb

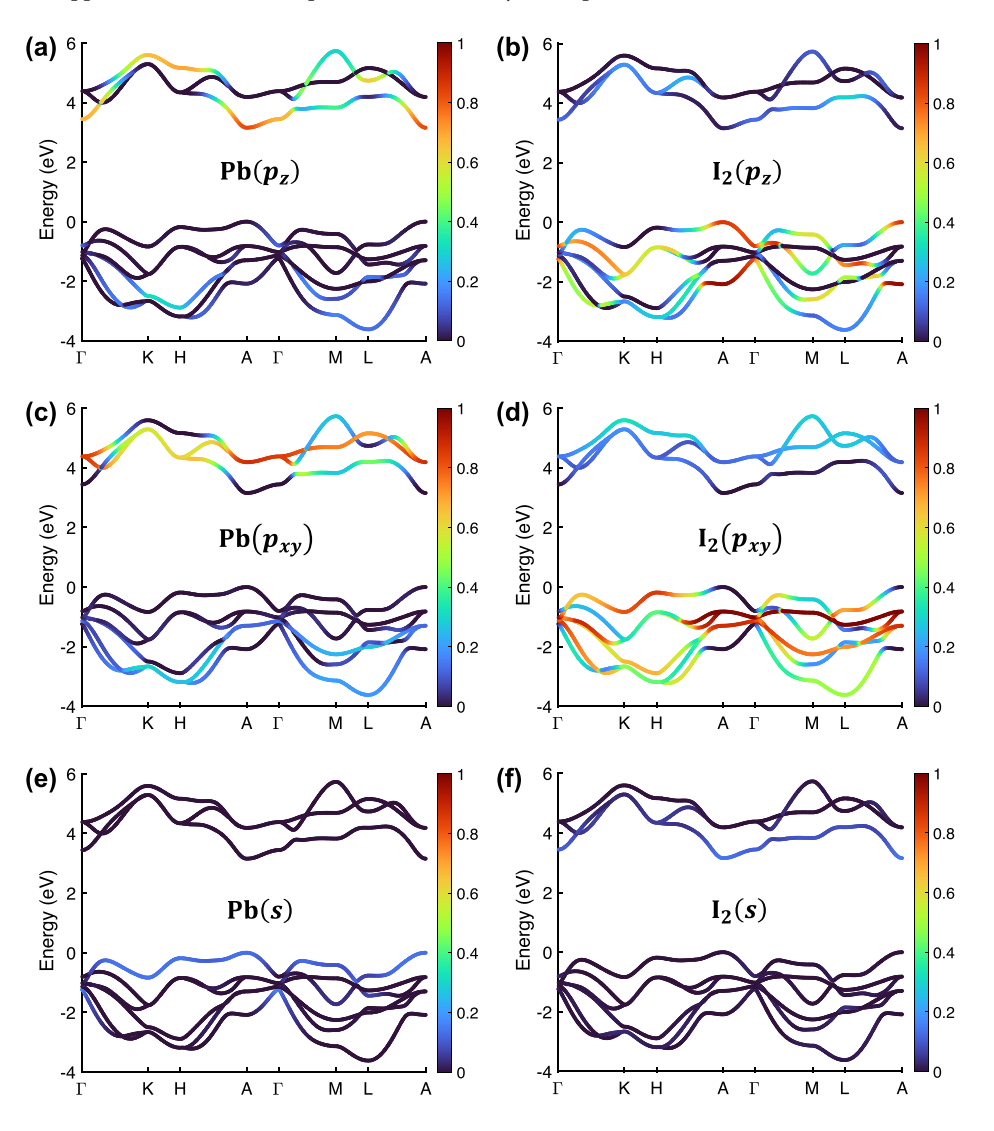


**FIG. 2.** State-projected band structure obtained from the scalar-relativistic pseudopotentials. Bloch wavefunctions are projected on the (a)  $p_z$  orbital of Pb atom, (b)  $p_z$  orbital of I atoms, (c)  $p_{xy}$  orbital of Pb atom, (d)  $p_{xy}$  orbital of I atoms, (e) s orbital of Pb atom, and (f) s orbital of I atoms. The values are normalized by the total projected density of states. The normalized PDOS indicate that the  $p_z$  orbitals of lead contribute to the bands near the CBM, while the bands near VBM mainly originate from the  $p_z$  orbitals of iodine.

contribute to the bands near the conduction band minimum while the 6s orbitals of Pb and the  $5p_z$  orbitals of I contribute to the bands near the valence band maximum. The next two conduction bands are derived from the  $6p_x$  and  $6p_y$  orbitals of Pb, while deeper valence bands are formed by the  $5p_x$  and  $5p_y$  orbitals of I.

However, the inclusion of the spin-orbit coupling leads to the mixing of the band orbital characters. As illustrated in Fig. 3, the characters of  $p_x$  and  $p_y$  orbitals of Pb are significantly enhanced for the conduction bands near the CBM, while the character of  $p_z$  orbital of Pb diminishes. Similarly, the characters of  $p_x$  and  $p_y$  orbitals of I are strengthened for the valence bands near the VBM, but the degree of band mixing is less significant than that of conduction bands near the CBM. Overall, these changes in band character indicate that SOC has a significant impact on the optical properties, which heavily depend on the characteristics of band edges.

Even though the band character analysis based on the orbital angular momentum provides a better understanding of the effect of SOC, we further investigate the total angular momentum j since the

orbital angular momentum l and the intrinsic spin angular momentum s are strongly coupled in PbI<sub>2</sub>. Correspondingly, we projected electron wavefunctions onto the eigenfunctions of the total angular momentum. We demonstrate that Pb 6p orbitals  $(j=0.5, m_j=\pm 0.5)$  mainly comprise the CBM, while I 5p orbitals  $(j=1.5, m_j=\pm 0.5)$  contribute to the VBM (Fig. S3). Due to the inversion symmetry and time-reversal symmetry, both the conduction band minimum and the valence band maximum of PbI<sub>2</sub> exhibit spin-degeneracy. Moreover, we observe the splitting of the conduction bands into the bands with j=3/2 and j=1/2, yielding a SOC gap of 0.93 eV at  $\mathbf{k}=A$  [Figs. S3(a) and S3(c)]. Such strong spin-orbit splitting is attributed to the heavy-element Pb atom and is also reported for lead halide perovskites.

The mixing of the band character is directly reflected in the change in the optical matrix elements. In Fig. 4, we plot the matrix elements of the momentum operator between the lowest conduction band and the highest valence band evaluated along high-symmetry directions. At the band extrema  $(\mathbf{k} = A)$ , if the SOC effect is not

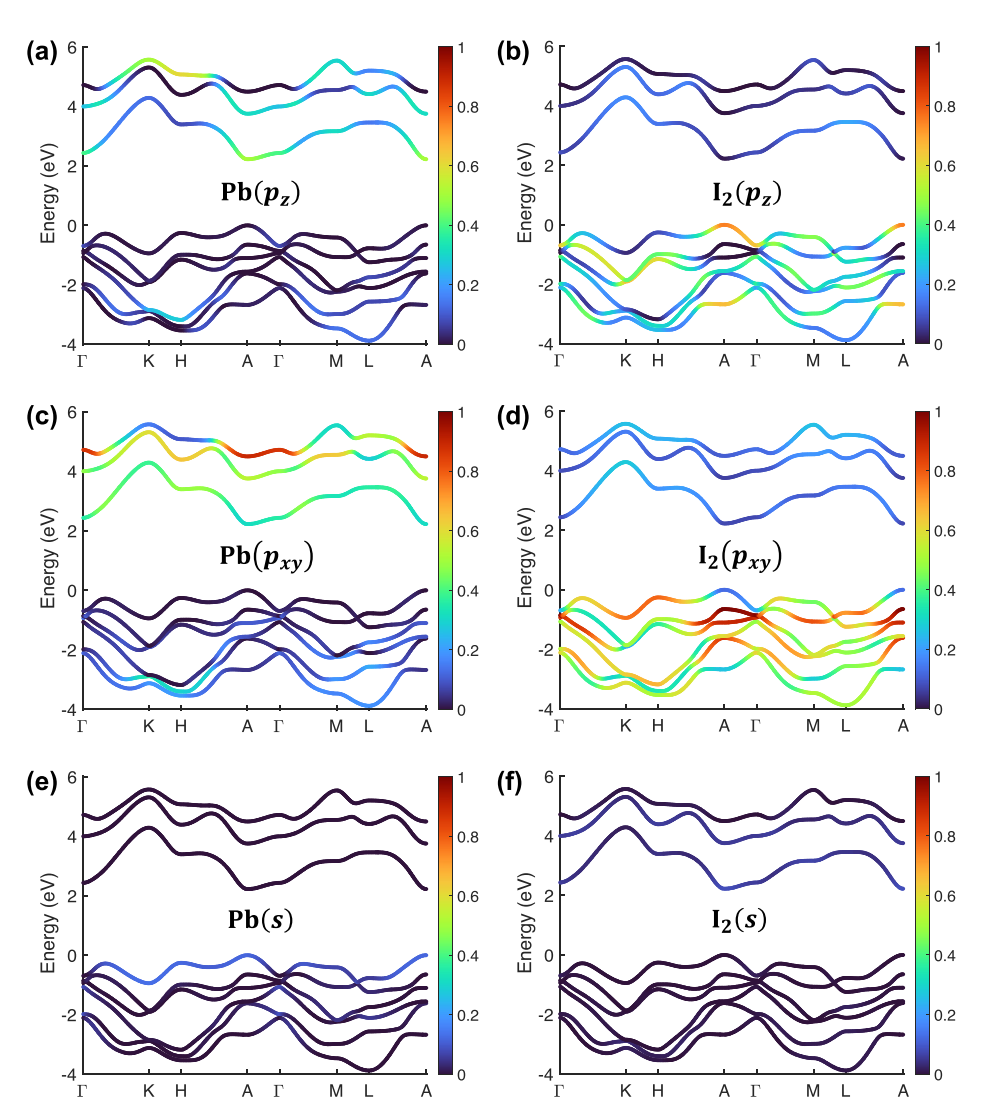


**FIG. 3.** State-projected band structure obtained from the fully-relativistic pseudopotentials. Bloch wavefunctions are projected on the (a)  $p_z$  orbital of Pb atom, (b)  $p_z$  orbital of I atoms, (c)  $p_{xy}$  orbital of Pb atom, (d)  $p_{xy}$  orbital of I atoms, (e) s orbital of Pb atom, and (f) s orbital of I atoms. The values are normalized by the total projected density of states. The normalized PDOS indicate that the SOC mixes the band characters and leads to the enhanced contribution from  $p_x$  and  $p_y$  orbitals for the bands near the band extrema.

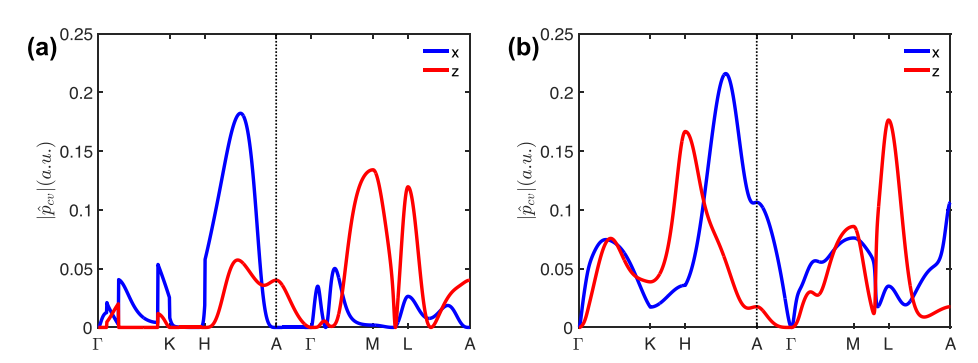


**FIG. 4.** Interband momentum matrix elements along high-symmetry directions evaluated without and with SOC. (a) Without SOC, the magnitude of the matrix elements at the band extrema ( $\mathbf{k} = A$ ) is strong for light polarization perpendicular to the Pbl<sub>2</sub> plane (i.e., along the z axis) and zero within the plane (x axis), indicating anisotropic optical properties. (b) When the SOC effect is included, the matrix element becomes nonzero for both polarizations, with the matrix element within the plane becoming much stronger than along the z axis, which indicates that orbital mixing by SOC enables dipole-forbidden transitions for light polarized within the Pbl<sub>2</sub> planes to become allowed.

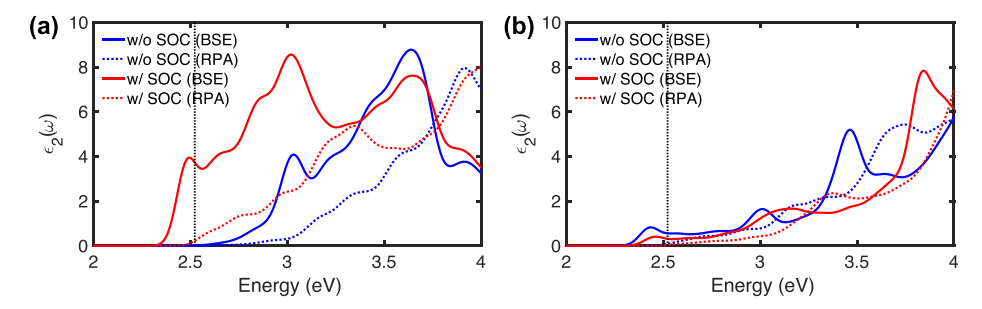


FIG. 5. Absorption spectrum of bulk Pbl<sub>2</sub> for (a) in-plane and (b) out-of-plane polarized light. Red and blue curves represent the absorption spectrum with and without SOC, respectively. For each case, the absorption spectrum is obtained with (BSE, solid lines) and without (RPA, dashed lines) the inclusion of excitonic effects. The electronic gap is set to 2.52 eV (vertical dashed line) for all the considered cases. Including spin–orbit significantly alters the overall absorption spectrum. Especially, the strong excitonic peak below the bandgap is observed for in-plane polarization only when SOC is considered, demonstrating the importance of SOC for the optical processes of Pbl<sub>2</sub>.

considered, the momentum matrix element shows a large value for light polarization along the out-of-plane direction while the value for the in-plane direction is zero [Fig. 4(a)]. Based on the band character analysis (Figs. 2 and 3), the optical transitions at the band extrema are dominated by the transitions between  $p_z$  orbitals of Pb and I atoms. However, we observe that the inclusion of SOC changes the transition probabilities due to the mixing of band characters [Fig. 4(b)]: in-plane transitions are enabled and relatively stronger than transitions along the out-of-plane direction. This should, therefore, result in strong optical absorption/emission peaks.

The effect of SOC on the band character and transition probability is also well-illustrated in the calculated absorption spectrum (Fig. 5). To concentrate on the influence of SOC and excitonic effect, we applied a rigid shift to fix the electronic gap for all the absorption calculations to  $2.52 \, \text{eV}$ . Without SOC, there are only dark exciton states below the electronic gap for the in-plane polarization [Fig. 5(a)]. This can be attributed to the  $p_z$ -character of the bands near CBM and VBM. Bright exciton states and corresponding strong absorption peaks are only observed for the higher energy range above the electronic gap. These bright exciton states are mainly composed of the transitions between higher-energy conduction bands and valence bands which show  $p_x$  and  $p_y$  band characters. On the other hand, we see an absorption peak below the electronic gap in the case of out-of-plane polarization. This absorption peak originates from the bright

exciton state that is mainly formed by the transitions near the band extrema ( $\mathbf{k}=A$ ). Therefore, we conclude that the strong absorption peak below the bandgap will only appear in the case of out-of-plane polarization when the SOC effect is not included.

However, with the inclusion of SOC, we observe completely different absorption spectra for in-plane and out-of-plane polarized cases (Fig. 5). For the case of in-plane polarization, the overall absorption spectrum shifts to the lower-energy due to the band mixing, and a bright excitonic peak appears below the bandgap. Meanwhile, the intensity of the excitonic absorption peak for the out-of-plane polarized light decreased, confirming the change of the band character. The trend corresponds well with the change in dipole matrix elements (Fig. 4).

In addition, SOC also affects the exciton binding energy. Table III shows that the inclusion of SOC leads to the reduction of the binding

**TABLE III.** Exciton binding energy calculated for in-plane and out-of-plane polarization. Inclusion of the SOC leads to a slight decrease in the exciton binding energy due to reduction in effective mass.

	w/o SOC	w/ SOC
$E_B(E \perp c)  E_B(E \parallel c)$	68.9 meV 98.5 meV	48.6 meV 83.3 meV

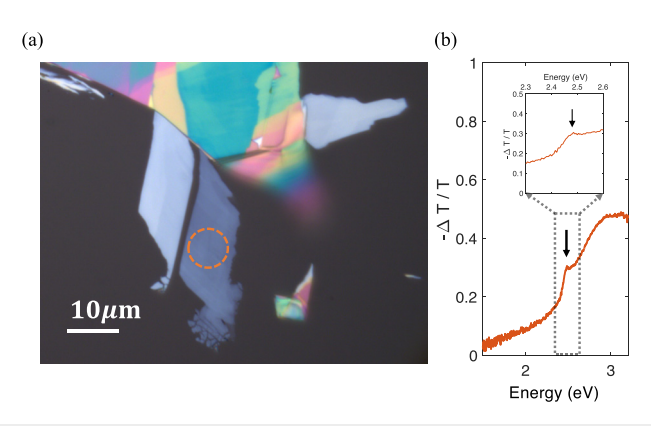


**FIG. 6.** (a) Optical image of a mechanically exfoliated Pbl<sub>2</sub> sample. The circled region corresponds to the measurement area. (b) Experimentally measured differential transmission spectrum of bulk Pbl<sub>2</sub>.

energy, which is mainly attributed to the large reduction in the hole effective mass along the in-plane direction (Table II). Our analysis indicates that the role of SOC is critically important to understand the optical transitions of bulk PbI<sub>2</sub>.

Finally, we calculated the absorption spectrum with randomphase approximation (RPA) to verify the importance of excitonic effects in PbI<sub>2</sub>. As illustrated in Fig. 5, there are large differences between the two absorption spectra obtained without (RPA, dashed curves) and with (BSE, solid curves) the inclusion of excitonic interactions. The overall transfer of spectral weight from high energies to low energies is attributed to the characteristic effect of excitonic corrections. Especially, the bright 1s exciton absorption peak below the electronic gap appears only when the excitonic effect is considered. Meanwhile, the absorption spectra obtained without the excitonic effect (RPA, dashed curves) show onsets at the electronic gap (2.52 eV, vertical dashed line). As a consequence, we conclude that both SOC and excitonic effects play a major role in optical processes in PbI<sub>2</sub>.

To further support our calculations, we measure differential transmission  $(-\frac{\Delta T}{T})$  of bulk PbI2 at room temperature. Here,  $-\frac{\Delta T}{T}=-\frac{(I_{\rm flake+subs}-I_{\rm subs})/I_{\rm flac}}{I_{\rm subs}/I_{\rm flac}}$  and is related to absorbance (A) by A  $=-\log_{10}(-\frac{\Delta T}{T})$ .  $I_{\rm inc}$ ,  $I_{\rm subs}$ , and  $I_{\rm flake+subs}$  correspond to the intensities of incident light, transmitted light after substrate only, and transmitted light after both substrate and flake, respectively. The circled area in Fig. 6(a) shows the measurement area (relatively large due to the large white light spot size). The uniformity of measurement area of the mechanically exfoliated samples was confirmed by atomic force microscopy (AFM) (Fig. S4) to rule out any thickness related contributions. Please refer to additional data corresponding to various thicknesses in the supplementary material (Fig. S5). The dominant absorption peak around 2.48 eV in Fig. 6(b) is in good agreement with the simulations [2.476 eV, Fig. 5(a)] and previously reported spectra.  $^{42-44}$ 

In conclusion, we demonstrate that SOC is of vital importance to the electronic and optical properties of PbI<sub>2</sub>. Our first-principles calculations based on density functional theory and many-body perturbation theory illustrate how SOC modifies the band character and the related electronic parameters, such as bandgap and carrier effective masses. Following calculations on momentum matrix elements and

absorption spectrum indicate that the fine structure of the exciton is strongly affected by the SOC and this change is directly reflected in the optical spectrum of PbI $_2$ . Our study provides an insight for fundamental processes of PbI $_2$  and its wide applications as optical materials and high-efficiency optoelectronic devices.

See the supplementary material for details on the deep-energy bands originating from the 6s orbital of Pb atoms, comparison between the calculation results with the semicore Pb pseudopotential and the valence Pb pseudopotential, projected density of states (PDOS) obtained from fully relativistic pseudopotentials, optical image and atomic force microscopy (AFM) data, and differential transmission spectra of bulk PbI<sub>2</sub>.

This work was supported through the National Science Foundation (NSF) (Grant No. DMR-1904541). Computational resources were provided by the National Energy Research Scientific Computing (NERSC) Center, a Department of Energy Office of Science User Facility supported under Contract No. DEAC0205CH11231. W.L. was partially supported by the Kwanjeong Educational Foundation Scholarship.

### AUTHOR DECLARATIONS Conflict of Interest

The authors have no conflicts to disclose.

#### **Author Contributions**

Woncheol Lee: Conceptualization (equal); Data curation (equal); Formal analysis (equal); Investigation (equal); Methodology (equal); Software (equal); Validation (equal); Visualization (equal); Writing original draft (equal); Writing - review & editing (equal). Zhengyang Lyu: Conceptualization (equal); Data curation (equal); Formal analysis (equal); Investigation (equal); Methodology (equal); Validation (equal); Writing - original draft (equal); Writing - review & editing (equal). Zidong Li: Conceptualization (equal); Data curation (equal); Formal analysis (equal); Investigation (equal); Methodology (equal); Validation (equal); Writing - review & editing (equal). Parag B. Deotare: Conceptualization (equal); Funding acquisition (equal); Project administration (equal); Resources (equal); Supervision (equal); Validation (equal); Writing - review & editing (equal). Emmanouil Kioupakis: Conceptualization (equal); Funding acquisition (equal); Project administration (equal); Resources (equal); Supervision (equal); Validation (equal); Writing – review & editing (equal).

#### **DATA AVAILABILITY**

The data that support the findings of this study are available from the corresponding author upon reasonable request.

#### **REFERENCES**

- <sup>1</sup>P. A. Beckmann, Cryst. Res. Technol. **45**, 455 (2010).
- <sup>2</sup>A. Ferreira Da Silva, N. Veissid, C. Y. An, I. Pepe, N. Barros De Oliveira, and A. V. Batista Da Silva, Appl. Phys. Lett. 69, 1930 (1996).
- <sup>3</sup>X. Liu, S. T. Ha, Q. Zhang, M. De La Mata, C. Magen, J. Arbiol, T. C. Sum, and Q. Xiong, ACS Nano 9, 687 (2015).
- <sup>4</sup>J. Zhang, T. Song, Z. Zhang, K. Ding, F. Huang, and B. Sun, J. Mater. Chem. C <sup>3</sup> 4402 (2015)

- <sup>5</sup>N. J. Jeon, J. H. Noh, W. S. Yang, Y. C. Kim, S. Ryu, J. Seo, and S. Il Seok, Nature 517, 476 (2015).
- <sup>6</sup>W. Chen, Y. Wu, Y. Yue, J. Liu, W. Zhang, X. Yang, H. Chen, E. Bi, I. Ashraful, M. Grätzel, and L. Han, Science 350, 944 (2015).
- <sup>7</sup>J. Zhang, Y. Huang, Z. Tan, T. Li, Y. Zhang, K. Jia, L. Lin, L. Sun, X. Chen, Z. Li, C. Tan, J. Zhang, L. Zheng, Y. Wu, B. Deng, Z. Chen, Z. Liu, and H. Peng, Adv. Mater. 30, 1803194 (2018).
- <sup>8</sup>Y. Sun, Z. Zhou, Z. Huang, J. Wu, L. Zhou, Y. Cheng, J. Liu, C. Zhu, M. Yu, P. Yu, W. Zhu, Y. Liu, J. Zhou, B. Liu, H. Xie, Y. Cao, H. Li, X. Wang, K. Liu, X. Wang, J. Wang, L. Wang, and W. Huang, Adv. Mater. 31, 1806562 (2019).
- <sup>9</sup>J. Xiao, L. Zhang, H. Zhou, Z. Shao, J. Liu, Y. Zhao, Y. Li, X. Liu, H. Xie, Y. Gao, J. T. Sun, A. T. S. Wee, and H. Huang, ACS Appl. Mater. Interfaces 12, 32099 (2020).
- <sup>10</sup> W. Zheng, B. Zheng, C. Yan, Y. Liu, X. Sun, Z. Qi, T. Yang, Y. Jiang, W. Huang, P. Fan, F. Jiang, W. Ji, X. Wang, and A. Pan, Adv. Sci. 6, 1802204 (2019).
- <sup>11</sup>D. Zhang, Y. Liu, M. He, A. Zhang, S. Chen, Q. Tong, L. Huang, Z. Zhou, W. Zheng, M. Chen, K. Braun, A. J. Meixner, X. Wang, and A. Pan, Nat. Commun. 11, 4442 (2020).
- <sup>12</sup>M. R. Tubbs and A. J. Forty, J. Phys. Chem. Solids 26, 711 (1965).
- <sup>13</sup>G. Harbeke and E. Tosatti, Phys. Rev. Lett. 28, 1567 (1972).
- <sup>14</sup>I. C. Schlüter and M. Schlüter, Phys. Rev. B **9**, 1652 (1974).
- <sup>15</sup>A. S. Toulouse, B. P. Isaacoff, G. Shi, M. Matuchová, E. Kioupakis, and R. Merlin, Phys. Rev. B 91, 165308 (2015).
- <sup>16</sup>M. Zhou, W. Duan, Y. Chen, and A. Du, Nanoscale 7, 15168 (2015).
- <sup>17</sup>M. F. Lin, M. A. Verkamp, J. Leveillee, E. S. Ryland, K. Benke, K. Zhang, C. Weninger, X. Shen, R. Li, D. Fritz, U. Bergmann, X. Wang, A. Schleife, and J. Vura-Weis, J. Phys. Chem. C 121, 27886 (2017).
- <sup>18</sup>Z. Y. Zhu, Y. C. Cheng, and U. Schwingenschlögl, Phys. Rev. B **84**, 153402 (2011).
- <sup>19</sup>G. Wang, C. Robert, A. Suslu, B. Chen, S. Yang, S. Alamdari, I. C. Gerber, T. Amand, X. Marie, S. Tongay, and B. Urbaszek, Nat. Commun. 6, 10110 (2015).
- <sup>20</sup>M. A. Becker, R. Vaxenburg, G. Nedelcu, P. C. Sercel, A. Shabaev, M. J. Mehl, J. G. Michopoulos, S. G. Lambrakos, N. Bernstein, J. L. Lyons, T. Stöferle, R. F. Mahrt, M. V. Kovalenko, D. J. Norris, G. Rainò, and A. L. Efros, Nature 553, 189 (2018).
- <sup>21</sup>P. C. Sercel, J. L. Lyons, D. Wickramaratne, R. Vaxenburg, N. Bernstein, and A. L. Efros, Nano Lett. 19, 4068 (2019).
- <sup>22</sup>P. Giannozzi, O. Andreussi, T. Brumme, O. Bunau, M. Buongiorno Nardelli, M. Calandra, R. Car, C. Cavazzoni, D. Ceresoli, M. Cococcioni, N. Colonna, I. Carnimeo, A. Dal Corso, S. de Gironcoli, P. Delugas, R. A. DiStasio, A. Ferretti, A. Floris, G. Fratesi, G. Fugallo, R. Gebauer, U. Gerstmann, F. Giustino, T. Gorni, J. Jia, M. Kawamura, H.-Y. Ko, A. Kokalj, E. Küçükbenli, M. Lazzeri,

- M. Marsili, N. Marzari, F. Mauri, N. L. Nguyen, H.-V. Nguyen, A. Otero-de-la-Roza, L. Paulatto, S. Poncé, D. Rocca, R. Sabatini, B. Santra, M. Schlipf, A. P. Seitsonen, A. Smogunov, I. Timrov, T. Thonhauser, P. Umari, N. Vast, X. Wu, and S. Baroni, J. Phys.: Condens. Matter 29, 465901 (2017).
- <sup>23</sup>D. M. Ceperley and B. J. Alder, Phys. Rev. Lett. **45**, 566 (1980).
- <sup>24</sup>J. P. Perdew and A. Zunger, Phys. Rev. B 23, 5048 (1981).
- <sup>25</sup>J. Deslippe, G. Samsonidze, D. A. Strubbe, M. Jain, M. L. Cohen, and S. G. Louie, Comput. Phys. Commun. 183, 1269 (2012).
- <sup>26</sup>M. S. Hybertsen and S. G. Louie, Phys. Rev. B **34**, 5390 (1986).
- <sup>27</sup>J. Deslippe, G. Samsonidze, M. Jain, M. L. Cohen, and S. G. Louie, Phys. Rev. B 87, 165124 (2013).
- <sup>28</sup>N. Marzari, A. A. Mostofi, J. R. Yates, I. Souza, and D. Vanderbilt, Rev. Mod. Phys. 84, 1419 (2012).
- <sup>29</sup>G. Pizzi, V. Vitale, R. Arita, S. Blügel, F. Freimuth, G. Géranton, M. Gibertini, D. Gresch, C. Johnson, T. Koretsune, J. Ibañez-Azpiroz, H. Lee, J.-M. Lihm, D. Marchand, A. Marrazzo, Y. Mokrousov, J. I. Mustafa, Y. Nohara, Y. Nomura, L. Paulatto, S. Poncé, T. Ponweiser, J. Qiao, F. Thöle, S. S. Tsirkin, M. Wierzbowska, N. Marzari, D. Vanderbilt, I. Souza, A. A. Mostofi, and J. R. Yates, J. Phys.: Condens. Matter 32, 165902 (2020).
- <sup>30</sup>M. Rohlfing and S. G. Louie, Phys. Rev. B **62**, 4927 (2000).
- <sup>31</sup>B. A. Barker, J. Deslippe, J. Lischner, M. Jain, O. V. Yazyev, D. A. Strubbe, and S. G. Louie, Phys. Rev. B **106**, 115127 (2022).
- <sup>32</sup>Z. Li, D. F. Cordovilla Leon, W. Lee, K. Datta, Z. Lyu, J. Hou, T. Taniguchi, K. Watanabe, E. Kioupakis, and P. B. Deotare, Nano Lett. 21, 8409 (2021).
- <sup>53</sup>R. Ahuja, H. Arwin, A. F. Da Silva, C. Persson, J. M. Osorio-Guillén, J. Souza De Almeida, C. M. Araujo, E. Veje, N. Veissid, C. Y. An, I. Pepe, and B. Johansson, J. Appl. Phys. **92**, 7219 (2002).
- 34T. Goto, J. Phys. Soc. Jpn. 51, 3 (1982).
- 35M. S. Skolnick and D. Bimberg, Phys. Rev. B 18, 7080 (1978).
- <sup>36</sup>T. Goto, S. Saito, and M. Tanaka, Solid State Commun. **80**, 331 (1991).
- <sup>37</sup>S. Saito and T. Goto, Phys. Rev. B **52**, 5929 (1995).
- <sup>38</sup>A. Dal Corso and A. M. Conte, Phys. Rev. B **71**, 115106 (2005).
- 39 M. S. Dresselhaus, G. Dresselhaus, and A. Jorio, Group Theory (Springer, 2008).
- 40 J. Even, L. Pedesseau, J. M. Jancu, and C. Katan, J. Phys. Chem. Lett. 4, 2999 (2013).
- <sup>41</sup>D. Giovanni, H. Ma, J. Chua, M. Grätzel, R. Ramesh, S. Mhaisalkar, N. Mathews, and T. C. Sum, Nano Lett. 15, 1553 (2015).
- 42J. B. Anthony and A. D. Brothers, Phys. Rev. B 7, 1539 (1973).
- <sup>43</sup>C.-X. Sheng, Y. Zhai, E. Olejnik, C. Zhang, D. Sun, and Z. V. Vardeny, Opt. Mater. Express 5, 530 (2015).
- 44V. Gulia and A. G. Vedeshwar, Phys. Rev. B 75, 045409 (2007).